Single-photon double ionization of He and Ne

Roger J. Bartlett and Peter J. Walsh

Los Alamos National Laboratory, Los Alamos, New Mexico 87545

Z. X. He, Y. Chung, E-M Lee, and James A. R. Samson

Behlen Laboratory of Physics, University of Nebraska, Lincoln, Nebraska 68588-0111

(Received 20 April 1992)

The photoionization branching ratio for double ionization has been measured from threshold to 800 eV for Ne and from threshold to 560 eV for He. Both sets of data have an initial rise from threshold, in general agreement with other published results, but the Ne data reach a plateau value above threshold in contrast to some of the other measurements and to the He data. The Ne data reach a value of approximately 13%, while the He data approach a value of approximately 4% before decreasing. A plateau in the He data was not reached in our measurements but may exist at higher energies. The photoionization cross section for double ionization has been extracted from the branching-ratio data.

PACS number(s): 32.80.Fb

I. INTRODUCTION

The interaction of photons with atomic systems has been studied for many years. These studies have produced a wealth of data that is useful in many areas of science and engineering and has led to a much deeper understanding of atomic physics. A very successful calculational approximation that can reproduce and extend much of this data is the one-electron model. In this model the electron-electron interactions are approximated by a potential that depends only on the coordinates of a single electron. Unfortunately, by averaging out these interactions or correlation effects, many significant phenomena are missed.

For certain photon energy ranges it is energetically possible to produce multiple ionization by a single photon. In one such phenomenon known as shake off, an inner-shell electron is removed by the photon and one or more other electrons are also removed by the sudden change in the core potential that is produced. It is also possible for the core hole to be filled by an outer electron with the subsequent emission of an Auger electron. In each case a multi-ionized ion is produced by a single photon. Although electron correlation plays a part in these interactions [1–4], it is not the dominant effect. However, in the case where a valence electron is removed by the photon and a second valence electron is also ejected, then electron-electron interactions play a major part. This is the situation for He and Ne in the energy range studied here, and it is a case that requires a more complex theoretical treatment than that provided by the one-electron model.

A number of authors [5–13] have studied these correlation effects by measuring the ratio of double to single ionization as a function of photon energy. The results of such measurements indicate the strength of the electron-electron interaction and can be compared with calculations in order to test their validity. Unfortunately there is over 50% variation among the reported data in the en-

ergy range from the double-ionization threshold to approximately 200 eV above the threshold. Even the shape of the curves varies significantly. Although it is not clear why such large variations in the data exist, it is clear that even small amounts of stray or harmonic light in the photon beam can cause large effects on the measured ratio. It is particularly important to eliminate any lower-energy stray light ($h\nu >$ energy of single ionization), for these photons can contribute significantly to the single-ionization process and reduce the ionization ratio, particularly in the range where the single- and double-ionization cross sections are small compared to their maximum value. This effect seems to appear in some of the literature data. Also, any charge state discrimination in the ion-state spectrometer will cause variations in the branching ratio.

Because of the large variations in the reported data and to carry the measurements to higher photon energies we have measured the ratio of the double- to the single-ionization cross section for He and Ne. We have made an effort to eliminate all nonmonochromatic light so that corrections for these effects are at worst small.

II. EXPERIMENTAL METHOD

Two separate independent experimental apparatus were used to acquire the data and verify the results. Although the details of apparatus and data-acquisition systems were different, the general approach used in the two systems was the same. Each setup consisted of a synchrotron-radiation photon source coupled to a monochromator. The photons from the monochromator were further filtered and then intercepted an effusive gas jet. The ions produced in the interaction volume were then analyzed and detected by a time-of-flight (TOF) ion-state spectrometer. The number of ions in each ionization state was recorded as a function of photon energy. A differential pumping section provided vacuum isolation between the monochromator and the sample chamber.

The system used on the Aladdin storage ring is essentially the same as that described in Ref. [12], with the exception that the length of the ion-state spectrometer was only 3 cm instead of 21 cm long and the start signal was obtained from the ring electrons operating in the single bunch mode. The system used at Aladdin differed mainly in the TOF ion-state spectrometer from that used at the National Synchrotron Light Source (NSLS), which is described below.

A. Photon source and filter systems

For the experiments performed at the National Synchrotron Light Source, the Los Alamos U3C beam line on the vacuum ultraviolet storage ring was used. The line is described elsewhere [14]. Briefly, light from the storage ring is focused in the horizontal plane onto the entrance slit of an ERG monochromator. The light was dispersed by either a 2-m radius 900-line/mm grating or a 5-m radius 1200-line/mm grating. The gratings were formed by the holographic ion etched process and had laminar groove shapes. This tended to reduce the amount of harmonic light present in the beam. With these gratings a photon energy range from approximately 25 to 1200 eV could be covered. The diverging light from the monochromator was focused onto the sample volume (spot size $\sim 3 \times 0.5$ mm^2) by a bent cylindrical mirror.

Thin-film filters could be inserted into the beam between the exit of the monochromator and the sample chamber. The filters were mounted on two wheels and could be rotated into the beam. The materials that were used and their thickness in micrograms per square centimeter were Be (1), B (1.5), C (5.3), Al (113), Ti (350), Cr (150), and Ni (673). All of these filters were effective in reducing the low-energy stray light, and had adequate transmission of the desired photons near but below the K or L absorption edges. To test the effectiveness of the filters, data were taken below and above the absorption edges. The small signal that existed above the edge was assumed to be due to higher harmonic light and was subtracted from the signal below the edge. This correction was always quite small (less than 3%). Essentially all of the data reported here were taken with one of the filters in the beam.

A low-pass filter consisting of two critical angle mirrors was also used to reduce the harmonic light in the beam. The filter consisted of two parallel mirrors spaced 0.5 cm apart. The beam out of the filter was parallel to the input beam but offset approximately 1 cm. Either a set of carbon-coated mirrors or a set of aluminum-coated mirrors could be inserted into the beam and the angle of incidence on the mirrors adjusted to set the cutoff photon energy. These adjustments could be made from outside the vacuum chamber.

The carbon mirrors could be set to have a minimum cutoff energy of approximately 124 eV, giving an effective harmonic free region down to ~ 62 eV. Under these conditions the filter throughput was about 25%. The aluminum-coated mirrors were used for energies above 350 eV. The cutoff energy for the carbon mirrors was fairly sharp, while that for the aluminum-coated mirrors was much more gradual.

B. Time-of-flight ion spectrometer

A schematic diagram of the time-of-flight ion spectrometer and the associated electronics is shown in Fig. 1. The design in many respects is similar to that used by Kossmann, Krassig, and Schmidt [15]. It consists of four regions where the ions are created, accelerated, and allowed to drift in a field-free region before reaching the detector. The regions are separated from each other by thin copper or copper-clad stainless-steel plates with center holes to allow for the ion transport. The holes are covered with 90% transparent copper mesh to minimize the field penetration from one region to another. In the first region the photon beam intersects the effusive gas jet and a pulsed field is applied to eject the ions into the second region. In the second region the ions are further accelerated by a second pulsed field and then enter a field-free drift region. Between the end of the drift tube and the microchannel plate detector (MCP), the ions are further accelerated to over 5200 V. This final acceleration increases the energy of the ions to a level where no charge state discrimination due to the MCP is seen. This was tested by measuring the ionization branching ratio as a function of this final acceleration voltage. The voltage was increased until the ratio reached a plateau value where further increases did not change the ratio.

The TOF dimensions and the pulsed voltages on the first two regions have been chosen according to the Wiley and McLaren criteria [16] in order to minimize the effects of a finite interaction volume. In practice the voltages are adjusted to minimize the pulse width of the ion signal. Generally pulse widths of less than 25 ns are obtained.

The pulse generator initiates the cycle by applying a negative high-voltage pulse to the accelerating grid of the TOF. The pulse has a relatively slow rise time of approximately 50 ns. Then approximately 400 ns later a 5-ns rise-time positive high-voltage pulse is applied to the interaction region. This pulse is also used as a start pulse for the time-to-digital converter (TDC). The delay between the pulses is necessary to allow for ringing in the signal channel, caused by the first pulse, to decay. Because of the matched termination for the pulse on the in-
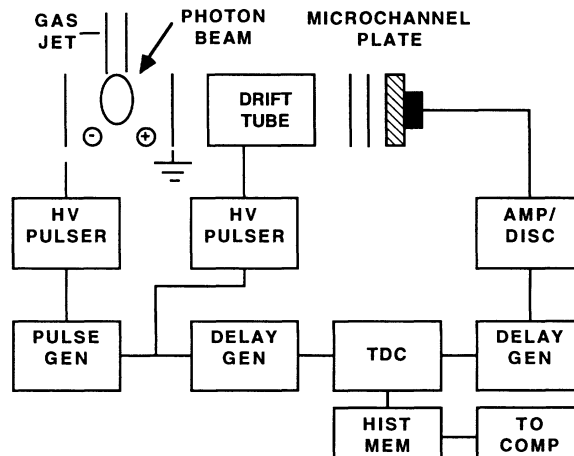
FIG. 1. Schematic diagram of the time-of-flight ion spectrometer and associated electronics used at the NSLS.

teraction volume very little ringing is caused by this second pulse. For lower pulse voltages the delay between the two pulses was reduced to zero without any measurable effect on the branching ratio. After a total time sufficient to eject and accelerate the lowest charge state ion, both pulses are returned to zero. After exiting the acceleration regions the ions drift to the end of the field-free region and are then accelerated to the MCP. The signal from the MCP is used to stop the TDC and the data in the TDC is transferred to a histogramming memory. The sequence is repeated for a preset time at each photon energy.

The maximum repetition frequency is limited by the electronic components in the system, or by the ion flight time and data-acquisition time. This limit is generally in the range from 100 to 330 kHz. At most one ion is detected during each cycle and this ion is the first to reach and be recorded by the detector. To account for multiple events during the cycle, Kossmann, Krassig, and Schmidt [15] have derived an expression that corrects exactly for this effect. However, for small count rates $NT \ll 1$, where N is the measured count rate and T is the cycle period, the correction is negligible. Corrections were never necessary for the experiments reported here.

To set the time delays, the histogramming memory, and TDC parameters, data were taken at a photon energy above the double-ionization threshold in order to see both the single- and double-ionization states. These data were taken with a TDC time resolution of 1.25 ns. After the initial set up, the data were then integrated to get the area under each ion peak and the ratio of the areas taken to determine the ratio of the two ion states. The TDC time resolution was then set to 40 ns per channel, a time greater than the full width of the ion peaks. In this mode the number of counts in each channel was equivalent to the area under the ion signal encompassed by that channel. The ratio of the ion states in this mode was just the ratio of the counts in the appropriate channels. The two methods give equivalent results. Mostly the latter method was used for data acquisition because of the simplicity gained by only having to divide the accumulated counts in the appropriate channels. This permitted a scanning mode of data collection to be used.

The sample gas was maintained at a fixed pressure in the range of 1.0 to 2.5×10^{-6} Torr by a feedback control system. To test for pressure effects the pressure was reduced by over a factor of 20 with no noticeable effect on the ion-state ratio. Thus no correction for pressure effects was required. The base pressure of the sample chamber prior to starting the flow of the sample gas was approximately 2×10^{-9} Torr.

The triple plus state of Ne could be seen above approximately 120 eV but its magnitude was insignificant compared to the other states. No correction for it has been made.

III. RESULTS AND DISCUSSION

A. Neon

The Ne data taken at the Synchrotron Radiation Center (SRC) (Aladdin storage ring) and at the NSLS

were combined. Agreement between the two sets of data was well within the variation in either set. No adjustments to either set of data were made. Because of the complete independence of the two measurements and the excellent agreement between them, we feel that this is a very good check on the accuracy of the results. The combined set of data extended from threshold (62.5 eV) to ~800 eV. From the measured ratio of the double-ionization cross section σ^{2+} to the single-ionization cross section σ^+, the branching ratio for double ionization σ^{2+}/σ_t was determined, where σ_t is the total ionization cross section. This was accomplished by dividing the measured ratio by 1 plus the ratio and assumes that the cross section is dominated by photoionization of the first two ionization states. This is the case in the energy range of interest here. This branching ratio is shown in Fig. 2.

In Fig. 3 the same data over a smaller energy range are compared with other measurements. There is a large variation in the reported values; however, we agree very well with the measurements of Schmidt et al. [7]. Our method of measurement is also quite similar to theirs, including the use of filters to reduce stray light in the photon beam. However, they only used a single polymer carbon filter and it is possible that some stray light still existed, causing a slight reduction in the branching ratio at the higher photon energies as seen in their last data point.

Carlson [5] used filtered x rays from a conventional x-ray source. This method was free from harmonic radiation but still was dependent on filtering for removal of the continuous radiation and unwanted line radiation. At threshold his data are on the high side of the various measurements, which may be due to averaging over a broad pass band on the steeply rising initial part of the double-ionization curve. However, at the higher energies (above those shown in Fig. 3), his data are in good agreement with ours.

Lightner, Van Brunt, and Whitehead [13] used filtered x-ray line radiation. They have one point from the K line of carbon that overlaps our data. The point at 280 eV has a value of 14.4% $\pm$ 1.5%. This is consistent with our data.
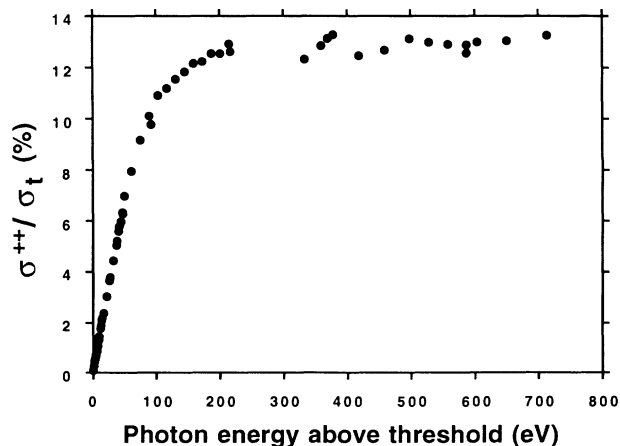
FIG. 2. Measured branching ratio of the double-photoionization cross section σ^{2+}/σ_t of Ne as a function of photon energy from threshold to approximately 800 eV.
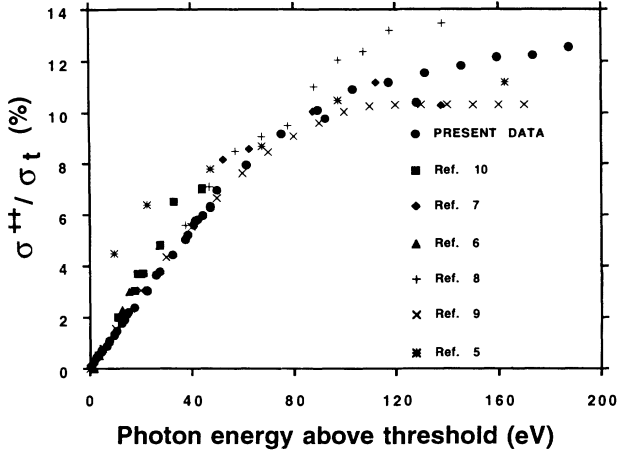
FIG. 3. Ne^{2+} branching ratio as a function of the photon energy above threshold. Present work compared with previously reported measurements.

TABLE I. Total and double-photoionization cross sections for Ne.

$h\nu$ (eV)	σ_t (Mb)	σ^{2+} (Mb)	$h\nu$ (eV)	σ_t (Mb)	σ^{2+} (Mb)
63.0	6.53	0.0070	345.0	0.276	0.0338
65.0	6.36	0.0269	360.0	0.248	0.0300
70.0	5.96	0.0619	375.0	0.220	0.0267
75.0	5.58	0.0982	390.0	0.192	0.0237
90.0	4.50	0.170	405.0	0.175	0.0218
105.0	3.57	0.208	420.0	0.160	0.0205
120.0	2.84	0.211	435.0	0.146	0.0192
135.0	2.24	0.201	450.0	0.131	0.0174
150.0	1.81	0.181	465.0	0.121	0.0156
165.0	1.51	0.163	480.0	0.112	0.0140
180.0	1.24	0.139	495.0	0.103	0.0129
195.0	1.04	0.121	510.0	0.0938	0.0118
210.0	0.884	0.106	525.0	0.0860	0.0110
225.0	0.780	0.0949	540.0	0.0802	0.0103
240.0	0.686	0.0845	555.0	0.0745	0.0097
255.0	0.593	0.0742	570.0	0.0690	0.0091
270.0	0.500	0.0634	585.0	0.0649	0.0085
285.0	0.429	0.0541	600.0	0.0611	0.0079
300.0	0.378	0.0481	615.0	0.0573	0.0074
315.0	0.332	0.0427	630.0	0.0535	0.0069
330.0	0.304	0.0380	645.0	0.0501	0.0063

Wight and Van der Wiel [8] used a pseudophoton method. They measured the energy loss of small-angle-scattered high-energy electrons in coincidence with the ions produced. This method does not suffer from either harmonic or stray light but may open other ionization channels if there is momentum transfer from the incident electron beam to the target atoms. This is possible if the scattering angle is not kept small. This may account for the somewhat higher branching ratio that they measure at the higher photon energies. It is also possible that their data is correct and indicates that all the other measurements are low due to stray light contamination.

The shape of the data of Holland et al. [9] agrees well with our measurements over the initial energy range, but the magnitude has been adjusted by a factor of 1.245. Their measuring technique was similar to ours, but they did not filter the photon source and relied on corrections to compensate for the stray light. This and several other correction factors may account for the discrepancy in the magnitude.

FIG. 4. Double-photoionization cross section of Ne as a function of photon energy from threshold to approximately 700 eV.

Any lower-energy light above the first ionization threshold will have large effects on the ionization ratio in the ranges where the cross section for single ionization is small. Stray light is believed to be the cause of the falloff in the branching ratio seen in the data of Samson and Angel [10]. Also any stray electrons created by the photon or electron probe can also preferentially ionize the sample. It is interesting to note that the results of Samson and Haddad [6] were obtained using a double-ionization chamber and a discrete line source. This arrangement eliminated the above-mentioned problems, including the problems of charge transfer and detector efficiency variations with ion state. The fact that their data agree with our results is further evidence that the stray and harmonic light in our measurements is adequately reduced.

The ionization ratio is theoretically expected to reach a plateau value for high photon energies [17–21]. Although it is not clear how high an energy is needed to reach this plateau, our data tend to level out at approximately 220 eV above the double-ionization threshold. However, the data are slightly increasing for increasing photon energies above this point to near the K edge, where a large increase is seen (not shown in the figures). This is not inconsistent with our view [11] that $\sigma^{2+}/\sigma_t \sim \sigma_e^+/\sigma_e$, where σ_e^+ is the cross section for single ionization of an ion by electron impact and σ_e is proportionality constant for a given atom. Rather, it implies that σ_e^+/σ_e also reaches a limiting value, which means that σ_e is decreasing as the energy above threshold increases. Even for a constant σ_e the proportionality holds from the double-ionization threshold to about 140 eV above it in the Ne case and holds over an even greater range for He as will be discussed below. The proportionality constant σ_e can be thought of as being an
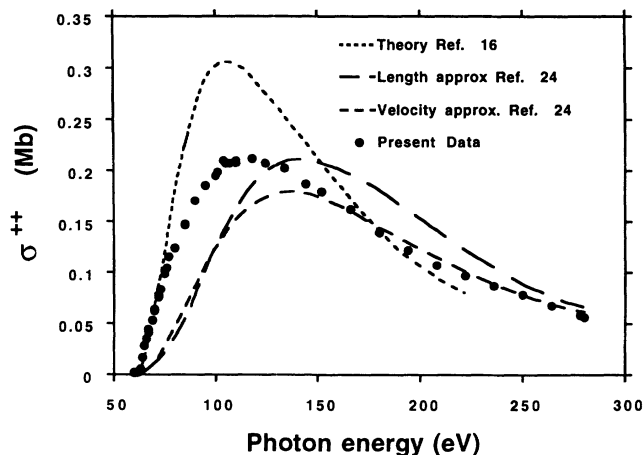
FIG. 5. Comparison between experiment and theory of the double-ionization cross section of Ne. The theoretical results are based on many-body perturbation theory.

FIG. 6. He^{2+} branching ratio as a function of photon energy above threshold. Present work compared with previously reported measurements.

effective collision cross section that brings the incident electron within the atomic dimensions of its target. Based on our data σ_e equals 318 Mb for Ne, which is consistent with an effective atomic diameter of ~ 2 Å.

We have extracted the double-ionization cross section from the measured ratio using the total ionization cross section of Samson and He [22] in the range from threshold to 144 eV, and Henke et al. [23] above 144 eV. The Samson and He data have an error of less than 2%. There is very good agreement between the two data sets over the entire overlap region of approximately 70 eV. In this energy range the Marr and West [24] data are approximately 13% higher but agree with the Henke data to within 5% in the range from 225 to 645 eV. The double-photoionization cross-section data are shown in Fig. 4 and are also tabulated in Table I along with values for the total ionization cross section used in the conversion.

Compared in Fig. 5 are the calculated cross sections of Chang and Poe [17] and those of Carter and Kelly [25] with the measured cross section. Over the initial part of the curve there is reasonable agreement with Chang and Poe [17], while above 150 eV there is better agreement with the velocity form of Carter and Kelly [25]. In these calculations a number of diagrams representing the many possible interaction channels in the atom are considered. It is possible that some interactions may be neglected or weighted incorrectly. For example, the participator Auger process as discussed by Becker et al [26] has been shown to lead to double ionization and will contribute over a portion of the energy range covered here. In general we believe the agreement with theory to be reasonable over portions of the energy range and that the comparison may lead to a better understanding of which interactions are dominant.

B. Helium

The measured double-ionization branching ratio for He is shown in Fig. 6 along with the data from several other authors [27–30]. Our data has been multiplied by a fac-

tor of 1.3 in order to compare the shape with the other measurements. The reason for the discrepancy in the absolute value of the data is not known; however, because of the low mass of He it is much more susceptible to the effects of stray fields and other perturbations in the apparatus. Our data agree quite well both in magnitude and shape with the calculations of Brown and Gould [18] and the shape is in agreement with the other measurements. As with Ne the double-photoionization cross section has been determined from the branching-ratio data and the total photoionization cross section of Samson and He [31]. The results are shown in Fig. 7.
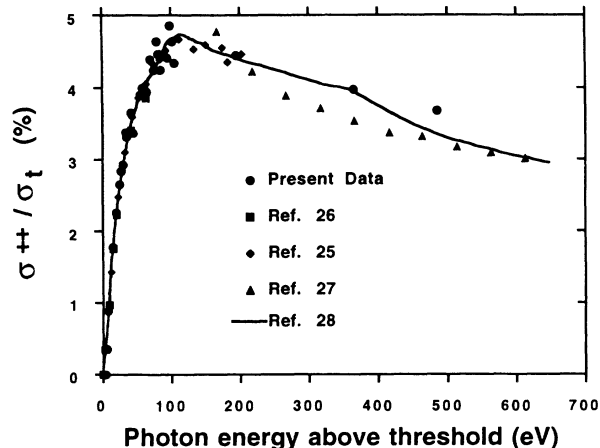
The He branching-ratio data reach a maximum around 125 eV above the double-ionization threshold and then decrease out to the limit of our measurements, approximately 560 eV. We do not see a plateau region in He as was found in Ne. The measurement of the ratio of the double to single photoionization of He at 2.8 keV by Levin et al. [32] gives a value 1.6%. This would indicate that the branching ratio is still decreasing beyond our measurements, but with a single point at 2.8 keV it is not
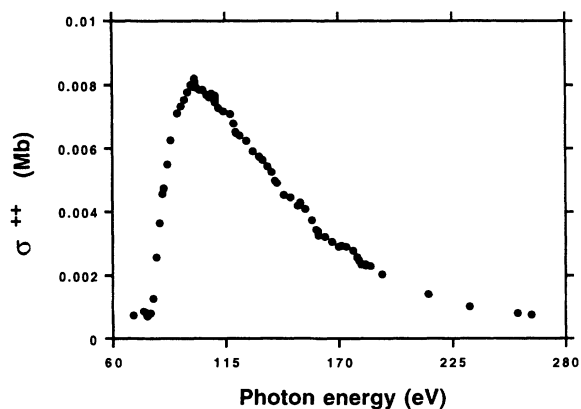
FIG. 7. Double-photoionization cross section of He as a function of photon energy from threshold to approximately 270 eV.

possible to say anything about the shape of the curve in that region.

As was mentioned the He data are consistent with the internal scattering model [11] and the electron-impact data of Peart, Walton, and Dolder [30] over the full range of the measurements. The relationship holds for a single proportionality constant σ_e of 98 Mb. This gives an effective atomic diameter of ~ 1 Å. At higher energies this effective collision cross section could decrease, thus σ^{2+}/σ_t may not decrease as rapidly as the electron-impact ionization data and in fact could reach a plateau.

IV. SUMMARY

The double-photoionization branching ratios for He and Ne have been measured from threshold to approximately 480 and 740 eV above threshold, respectively.

The Ne data reach a plateau ~ 220 eV above threshold, while the He data go through a maximum and decrease over the upper range of the measurements. The data are consistent with an internal scattering model proposed by Samson [11] and reported electron-impact ionization data of the singly charged ions.

[1] G. B. Armen, T. Aberg, K. R. Karim, J. C. Levin, B. Crasemann, G. S. Brown, M. H. Chen, and G. E. Ice, Phys. Rev. Lett. **54**, 182 (1985).

[2] W. Jitschin, U. Werner, G. Materlitz, and G. D. Doolen, Phys. Rev. A **35**, 5038 (1987).

[3] Svante Svensson, Bengt Eriksson, Nils Martensson, Goran Wendin, and Ulrik Gelius, J. Electron Spectrosc. and Relat. Phenom. **47**, 327 (1988).

[4] T. Aberg, Ann. Acad. Sci. Fenn. Ser. A6 **308**, 1 (1969).

[5] T. A. Carlson, Phys. Rev. **156**, 142 (1967).

[6] J. A. R. Samson and G. N. Haddad, Phys. Rev. Lett. **33**, 875 (1974).

[7] V. Schmidt, N. Sander, H. Kuntzemuller, P. Dhez, F. Wuilleumier, and E. Kallne, Phys. Rev. A **13**, 1748 (1976).

[8] G. R. Wight and M. J. Van der Wiel, J. Phys. B **9**, 1319 (1976).

[9] D. M. P. Holland, K. Codling, J. B. West, and G. V. Marr, J. Phys. B **12**, 2465 (1979).

[10] J. A. R. Samson and G. C. Angel, Phys. Rev. A **42**, 5328 (1990).

[11] J. A. R. Samson, Phys. Rev. Lett. **65**, 2861 (1990).

[12] J. A. R. Samson, G. N. Haddad, and L. D. Kilcoyne, J. Chem. Phys. **87**, 6416 (1987).

[13] G. S. Lightner, R. J. Van Brunt, and W. D. Whitehead, Phys. Rev. A **4**, 602 (1971).

[14] R. J. Bartlett, W. J. Trela, F. D. Michaud, S. H. Southworth, R. Rothe, and R. W. Alkire, Proc. SPIE **689**, 200 (1986).

[15] H. Kossmann, B. Krassig, and V. Schmidt, J. Phys. B **21**, 1489 (1988).

[16] W. C. Wiley and I. H. McLaren, Rev. Sci. Instrum. **26**, 1150 (1955).

[17] T. N. Chang and R. T. Poe, Phys. Rev. A **12**, 1432 (1975).

[18] R. L. Brown and R. J. Gould, Phys. Rev. D **1**, 2252 (1970).

[19] R. L. Brown, Phys. Rev. A **1**, 341 (1970).

[20] F. W. Bryon and C. J. Joachain, Phys. Rev. **164**, 1 (1967).

[21] J. H. McGuire, J. Phys. B **17**, L779 (1984).

[22] J. A. R. Samson and Z. X. He (unpublished).

[23] B. L. Henke, P. Lee, T. J. Tanaka, R. L. Shimabukuro, and B. K. Fujikawa, At. Data Nucl. Data Tables **27**, 1 (1982).

[24] G. V. Marr and J. B. West, At. Data Nucl. Data Tables **18**, 497 (1976).

[25] S.L. Carter and H. P. Kelly, Phys. Rev. A **16**, 1525 (1977).

[26] U. Becker, R. Wehlitz, O. Hemmers, B. Langer, and A. Menzel, Phys. Rev. Lett. **63**, 1054 (1989).

[27] J. M. Bizau, F. Wuilleumier, D. Ederer, P. Dhez, S. Krummacher, and V. Schmidt, as quoted by S. L. Carter and H. P. Kelly, Phys. Rev. A **24**, 170 (1981).

[28] H. Kossmann and V. Schmidt (private communication), as reported in Ref. [11].

[29] M. Ya Amusia, E. G. Drukarev, V. G. Gorshkov, and M. P. Kazachkov, J. Phys. B **8**, 1248 (1975).

[30] B. Peart, D. S. Walton, and K.T. Dolder, J. Phys. B **2**, 1347 (1969).

[31] J. A. R. Samson and Z. X. He (unpublished).

[32] J. C. Levin, D. W. Lindle, N. Keller, R. D. Miller, Y. Azuma, N. Berrah Mansour, H. G. Berry, and I. A. Sellin, Phys. Rev. Lett. **67**, 968 (1991).